Geochemical Perspectives Letters

The direct observation and interpretation of gas hydrate decomposition with ocean depth

L. Ma[1,2,3], Z. Luan[1,2,3], Z. Du[1,2], X. Zhang[1,2,3], Y. Zhang[1,2,3], X. Zhang[1,2,3*]

OPEN ACCESS

https://doi.org/10.7185/geochemlet.2327

Abstract

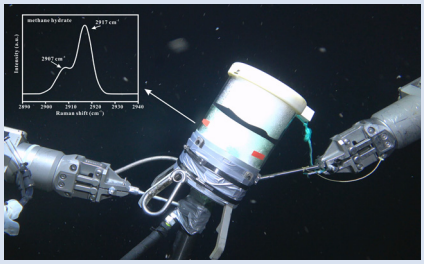

An exposed gas hydrate (EGH) evolutional model as a function of water depth was established by *in situ* EGHs ascent experiments in cold seep areas of Haima (1509 m, 2.88 °C and 15.22 MPa), Lingshui (1760 m, 2.56 °C, 17.76 MPa and pH = 7.97) and Site F (1100 m, 3.57 °C, 11.09 MPa and pH = 7.69) in the South China Sea. A remotely operated vehicle was used to reproduce the *in situ* EGH ascent. Changes and temperature variations during EGH ascent were monitored in real time using a Raman insertion probe and dissolved oxygen sensor. The EGH ascent involved three stages of change: i) the metastable stage where no morphology changes, but where gas escapes and there is a decrease in internal temperature; ii) a second stage of coexistence of peripheral hydrate decomposition and internal hydrate growth; iii) a third stage of internal hydrate decomposition at shallower depths. Experimental results indicated that EGHs can carry gas bubbles to shallow depths and even to the sea surface. This could be an important transport mode for cold seep gases affecting shallow waters or the atmosphere.

Received 21 April 2023 | Accepted 1 August 2023 | Published 1 September 2023

Introduction

Exposed gas hydrates (EGHs) have been frequently reported in shallow surface sediments, and are common beneath authigenic carbonate rocks and empty mussel shells in active cold seeps (Fig. 1) (Sassen *et al.*, 2004; Pohlman *et al.*, 2005; Hester *et al.*, 2007). EGHs are formed by the accumulation of rising methane bubbles, which are rapidly covered with hydrate film. These EGHs contain a large amount of free methane gas and have a soft and loose structure, representing the initial state of hydrate formation (Zhang *et al.*, 2017a; Du *et al.*, 2018). Disturbances such as submarine turbidity currents, processes related to climate change, and geological activity can cause the ascent of EGHs due to destabilisation (Rehder *et al.*, 2009). Rising decomposition may occur when EGHs are destabilised, but thermodynamic conditions in the deep ocean environment have the potential to convert the gas back to hydrates (Zheng *et al.*, 2020). The complex marine environment makes it difficult to predict the fate of EGHs in the natural state after destabilisation occurs and they escape into seawater. Previous research has shown that methane fluid from cold seep vents can be dissolved into the water column or consumed by methanotrophic microorganisms (Thornton *et al.*, 2016; Egger *et al.*, 2018). It is unknown whether EGHs destabilised into seawater can improve the survival ability of methane gas, and the depths to which EGHs can carry methane gas after a destabilised ascent remain uncertain.

The investigation of the hydrate evolution after their initial formation has been conducted *via* laboratory simulations in recent decades (Zhong *et al.*, 2016; Lei *et al.*, 2019). The morphology, thickening pattern, and growth resistance of hydrate film have been explored in detail (Zeng *et al.*, 2019; Qureshi *et al.*, 2022a; Dhamu *et al.*, 2023). Research conducted on hydrates in laboratories has typically been limited to steady-state systems at specific temperature and pressure conditions. Laboratory techniques are unavailable for use in real and complex ocean environments (Brewer *et al.*, 1998; Warzinski *et al.*, 2014). Compared to freshwater environments in the laboratory, EGHs in the marine environment are more unstable due to factors such as salinity and currents (Qureshi *et al.*, 2022b, 2022c). With the development of underwater vehicle technology and the increase in our understanding of cold seep regions, *in situ* technologies that can more accurately analyse natural gas hydrates have gradually matured. Initially, Brewer *et al.* (1998) made detailed recordings of the formation and growth patterns of gas hydrates as a function of depth, using a remotely operated vehicle (ROV). Hester *et al.* (2009) concluded that mass-transfer is the rate-controlling mechanism for the dissolution of EGHs and recorded the *in situ* decomposition of EGHs located in the Barkley Canyon area, off Vancouver Island, Canada. Recently, Du *et al.* (2018) characterised the structural features and evolution process of EGHs using Raman spectroscopy in the cold seep area of the South China Sea. A series of investigations of hydrate formation processes and their natural evolution have been performed through *in situ* experiments in recent decades. One similarity

1. Key Laboratory of Marine Geology and Environment & Center of Deep Sea Research, Institute of Oceanology, Center for Ocean Mega-Science, Chinese Academy of Sciences, Qingdao 266071, China
2. Laboratory for Marine Geology, LaoShan Laboratory, Qingdao 266061, China
3. University of Chinese Academy of Science, Beijing 100049, China
* Corresponding author (Email: xzhang@qdio.ac.cn)

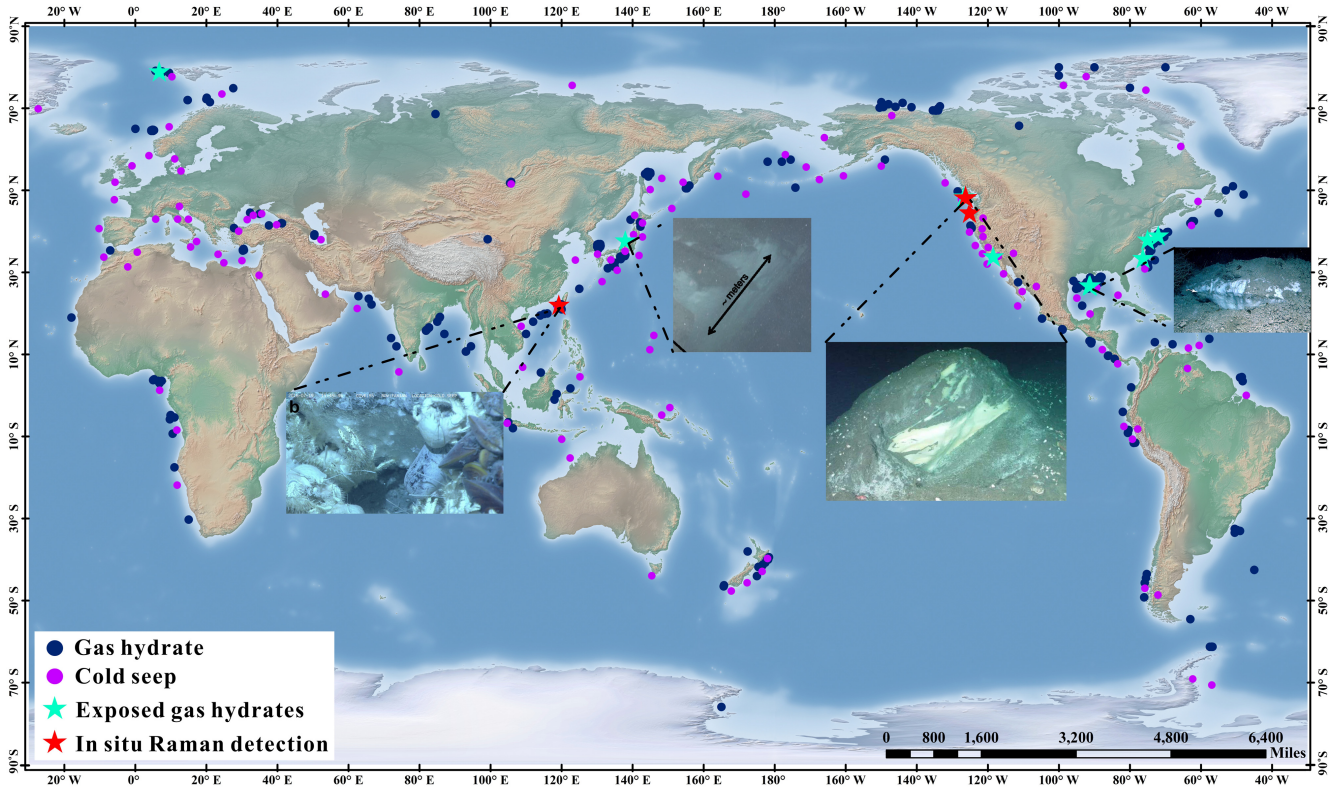

Figure 1 Global map of gas hydrates (Kvenvolden, 1988; Waite *et al.*, 2020) and cold seeps (Mazurenko and Soloviev, 2003; Suess, 2014). Cyan stars represent the locations of exposed gas hydrate occurrence (MacDonald *et al.*, 2003; Sassen *et al.*, 2004; Pohlman *et al.*, 2005; Roberts *et al*, 2006; Hester *et al.*, 2007; Case *et al.*, 2017). Red stars indicate locations where *in situ* Raman investigations of exposed hydrates have been performed (Hester *et al.*, 2007; Zhang *et al.*, 2017a).

among all these *in situ* experiments was that they were conducted in stationary environments, and there were no records obtained of EGHs as they rose to the surface. Thus, the evolution of EGHs during their rise is not yet clear.

In this study, we performed *in situ* experiments on the ascent decomposition of EGHs in the Haima, Lingshui, and Site F cold seep areas in the South China Sea (SCS) (Fig. 2a). The EGH samples were formed directly using gas-rich fluids that erupted from cold seep vents (Video S-1). We monitored the morphological changes that occurred during the EGH ascent using a camera mounted on the remotely operated vehicle (ROV) "*Faxian*" (Fig. 2b–g). A Raman insertion probe for gas hydrates (RiP-Gh), previously developed by Zhang *et al.* (2017b), and a dissolved oxygen sensor (DOS, JFE RINKO I ARO-USB) were used to capture the kinetic and thermodynamic behaviour of EGHs during their ascent (analytical methods are provided in detail in the Supplementary Information). Here, we report data from the *in situ* ascent of EGHs in a natural environment and analyse the corresponding impact on the upper water layers.

In Situ Raman Spectra of Exposed Gas Hydrate Samples

The Raman spectral data indicated that the gaseous component of the cold seep fluids consisted primarily of methane gas (Fig. S-1). When conducting the *in situ* experiments using cold seep vent fluids in the seafloor, we found that the formation of hydrates occurred nearly instantaneously (Video S-1). Methane gas bubbles were rapidly wrapped with a hydrate film during their ascent, which provided separation between the internal gas and external water (Fig. 2h). Multiple bubbles carrying hydrate films accumulated in cells to form a honeycomb structure in the EGH sample (Video S-1, Fig. 2h$_1$). After a stationary period, an RiP-Gh probe was inserted into the EGH sample at approximately 20 cm for *in situ* Raman spectral observation (Videos S-2 to S-4). Notably, the time that hydrates remained on the seafloor after formation varied in each *in situ* experiment. Hydrate samples remained on the seafloor for half an hour at the Haima cold seep, 2.6 hours at the Lingshui cold seep and 48 hours at the Site F cold seep (Table S-2). The different stationary periods of hydrates make our experiments more generalisable.

The Raman spectra of EGHs indicated two apparent Raman peaks occurring at 2907 cm^{-1} and 2917 cm^{-1}. Both Raman spectra and the guest molecule species indicated that the EGHs in our *in situ* experiments were all type I structures. Notably, the peak intensity at 2907 cm^{-1} was less than that at 2917 cm^{-1} (Fig. S-2). The Raman peak located at 2917 cm^{-1} consisted of a composite peak that was influenced by both a small cage vibration and the gaseous CH_4 vibration.

Stage Changes in the Rising Process of Exposed Gas Hydrates

In the Haima *in situ* experiments, the entire monitoring time of the rising EGHs was 0.79 h. There were three significant stage changes during the rising of the EGHs towards the surface (Video S-2). The first stage occurred at pressures of 15.22–7.05 MPa (1509–700 m). There were no significant changes in the morphology of the EGHs during this stage (Fig. S-3). However, the 2917 cm^{-1} composite peak intensity exhibited a decreasing trend, which was associated with the free CH_4 gas escaping as the hydrate migrated towards the surface

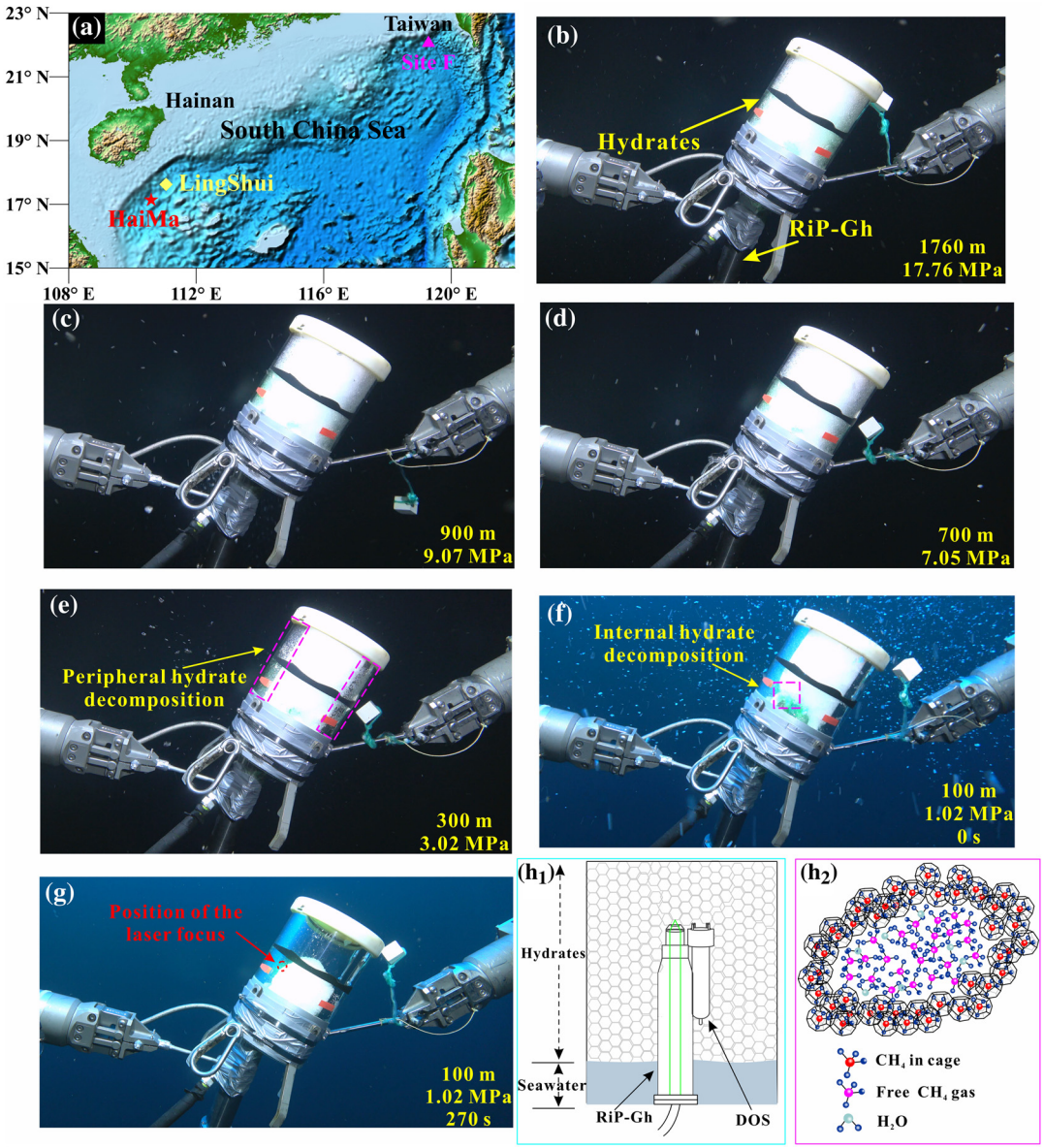

Figure 2 **(a)** Map showing the locations of the Haima, Lingshui and Site F cold seep vents. **(b–g)** Images showing hydrate collection and monitoring controlled by the ROV manipulator in Lingshui *in situ* experiment. **(h_1)** Schematic diagram of the RiP-Gh and DOS probes touching and being inserted into the EGHs for dynamic monitoring. **(h_2)** Schematic diagram of the hydrate film formed in the gas bubbles.

(Fig. 3b). In normal circumstances, the further growth of the hydrate can only occur *via* the diffusion of water molecules through the hydrate film, which occurs slowly (Dhamu *et al.*, 2023). However, during the ROV ascent, the hydrate film can rupture due to the decrease in pressure exerted by the seawater. Consequently, the gas inside the EGH samples will escape, leading to an accelerated exchange with water molecules and other surrounding media. In contrast, the peak intensity that occurred at 2907 cm^{-1} showed a weaker enhancement trend (Fig. 3b). Simultaneously, the large cage vibration after Gaussian fitting also shows an enhanced trend (Fig. 4a). This indicates the growth of the EGH samples at this stage. By comparing the hydrate stability curves, we found that the internal environment of the EGHs was consistent with the stable existence of hydrates (Fig. 4b).

The second stage occurs at pressures of 7.05–2.59 MPa (700–257 m) during the ascent. At this stage, the composite peak at 2917 cm^{-1} also shows a decreasing trend (Fig. 3b), indicating that the gas escapes. Raman spectral data suggest that the gas escapes throughout the experiment (Fig. 3a). The same process was also observed in the *in situ* experiments conducted at Lingshui and Site F (Figs. S-5 and S-6). The hydrate samples started decomposing from the periphery boundary at a pressure of approximately 7.05 MPa (700 m), when the ambient temperature of the seawater was 6.9 °C (Fig. 4a). The hydrate stability curve (Dickens and Quinby-Hunt, 1994) shows that the theoretical depth at which the decomposition of the EGHs begins is at the pressure of 6.19 MPa (614 m) (Fig. 4b). Here, the depth where decomposition of the EGH sample occurred was advanced during the ascent. Noticeably, although the EGH sample started to decompose from the periphery boundary, there was also a continued increase in the Raman intensity of the large cage inside of the EGHs (Fig. 4a). This suggests that there exists a continued growth inside the EGHs. Moreover, the temperature and pressure conditions inside the EGHs at this stage were consistent with the stable existence of hydrates (Fig. 4b). We monitored the continued hydrate growth process up to a pressure of 2.59 MPa (257 m) (Fig. 4a).

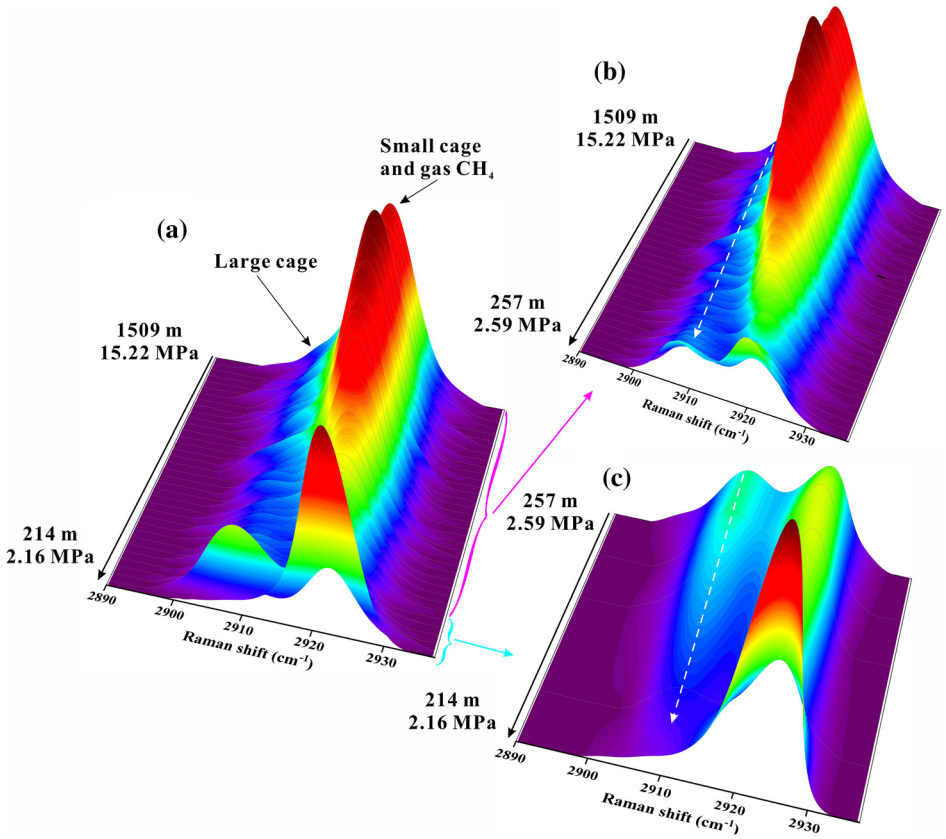

Figure 3 *In situ* Raman spectra for EGHs during their ascent towards the surface in the Haima cold seep. **(a)** Overall ascent over the pressure range of 15.22–2.16 MPa (1509–214 m). **(b)** The continuous growth stage at a Raman intensity of 2907 cm^{-1}, and the continuous decrease at 2917 cm^{-1}. **(c)** Hydrate decomposition stage.

The third stage occurs at pressures of 2.59–2.16 MPa (257–214 m) during the ascent. At this stage, the peak intensity at 2907 cm^{-1} and the large cage vibration (2905 cm^{-1}) abruptly decreased, indicating that the inside of the EGHs sample started to decompose (Figs. 3c and 4a). At a pressure of 2.16 MPa (214 m), the Raman signal of the hydrate disappeared, and only gaseous CH_4 remained (Fig. 3c). One interesting point we observed is that internal hydrate decomposition started at 2.59 MPa (257 m) during this stage. However, the hydrate equilibrium curve shows that the temperature and pressure inside the EGHs did not satisfy the conditions for the stable existence of EGHs as early as 3.34 MPa (332 m) (Fig. 4b). This indicates that the peripheral hydrate decomposition causes a hysteresis effect on the internal hydrate decomposition. Notably, at a pressure of 2.16 MPa (214 m), the complete decomposition of EGHs was recorded by the RiP-Gh probe. The residue of the EGHs, however, was still present above the sample cell.

The above data and discussions are based on the experiment conducted at the Haima cold seep vent. The *in situ* experiments conducted at Site F (Video S-4) and the Lingshui cold seep (Video S-3) vent locations also showed similar results to those at the Haima cold seep vent. The monitoring time for the rising process of EGHs in the Site F cold seep area was 0.61 h, while in the Lingshui cold seep area the monitoring time was 1.34 h. There were also three distinct stage changes during the EGH ascent (Figs. S-3 to S-7). During the *in situ* ascent experiment performed at Site F, the first stage occurred at pressures of 11.09–7.05 MPa (1100–700 m), the second stage occurred at pressures of 7.05–0.65 MPa (700–65 m), and the third stage occurred at pressures of 0.65–0.28 MPa (65–27 m) (Fig. S-7b). The first stage of the *in situ* experiment conducted at the Lingshui cold seep vent occurred at pressures of 17.76–7.05 MPa (1760–700 m) during the ascent process, and the second stage occurred at pressures of 7.05–1.01 MPa (700–100 m) (Fig. S-7a). The ROV did not continue to ascend in the third stage during the *in situ* experiment performed at the Lingshui cold seep vent. The ROV instead remained stationary at a water depth of 100 m (1.01 MPa), and we monitored the hydrate decomposition process of the third stage over time (Fig. S-7a). The third stage of the *in situ* experiment for the Lingshui cold seep vent lasted approximately 270 s (Fig. S-7a).

Specific Temperature Variations Inside Hydrates

The temperature of the EGHs showed a distinct trend from that of seawater. This appeared inconsistent with both the commonly believed exothermic and absorbed nature of hydrate formation and decomposition. In the first stage, the internal temperature of the hydrate samples dropped by 2.7 °C when the ambient temperature-pressure conditions fit the zone of hydrate stability (Fig. 4b). The ambient temperature of the seawater increased by 4 °C. At this stage, the hydrate periphery had not yet begun to dissipate, thus protecting the internal temperature of the gas hydrate from the influence of the ambient temperature of the seawater. The decrease in internal temperature was attributed to the dissolution of EGH samples. Various factors, such as the high methane chemical potential in the sample cell, the presence of oxygen, and the unsaturated methane concentration in the seawater, are likely reasons contributing to the dissolution of the EGHs.

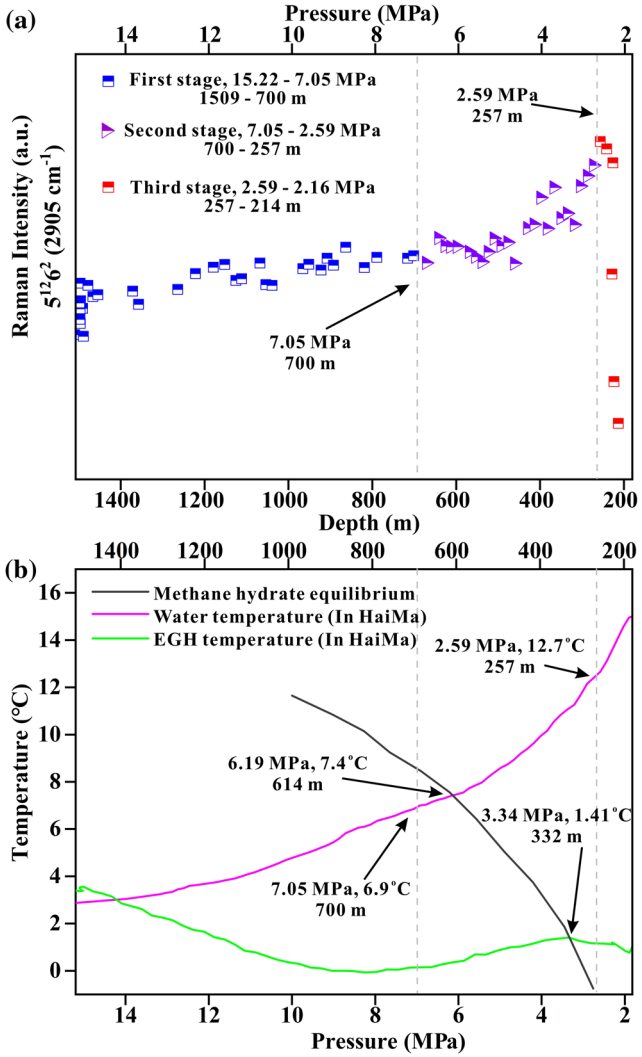

Figure 4 **(a)** Variation in the large cage Raman intensity with pressure during EGH ascent. **(b)** Temperature-pressure conditions present in the ambient seawater and the interior of the hydrate during EGH ascent. The black curve represents the phase equilibrium conditions for methane hydrate in seawater (S = 35 ‰) (Dickens and Quinby-Hunt, 1994).

However, when the EGH samples decomposed at the periphery boundary during the second stage, the internal temperature increased by 1.02 °C (Fig. 4b), and the temperature of the ambient seawater increased by 5.7 °C. During this stage, the inner environment of the hydrate was gradually exposed due to the periphery of the EGHs decomposing. The influence of seawater ambient temperature on the internal area of the hydrates intensified. The increase in the EGH inner temperature was likely influenced by the wide variation in the ambient temperature of the seawater. In the third stage, an approximately 1.5 °C increase in ambient temperature occurred at water depths of 257–214 m. Since the third stage only spanned 43 m, the influence of the ambient temperature of the seawater on the internal hydrates was small. The EGH internal temperature decreased by 0.31 °C at this stage due to the hydrate decomposition and endothermic processes.

New Insights into the Vertical Spreading of Bubbles in Cold Seep Areas

The depth of the location at which the Raman signal disappeared during the third stage represents the complete EGH decomposition. We estimated the variation in the hydrate volume with depth in the sample cells (Fig. S-8). All experiments showed that the gas hydrate was still retained above the sample cell at the end of the third stage. The rate of gas hydrate decomposition during the third stage was the fastest. The gas hydrate decomposition rates of the third stage in our three *in situ* experiments were estimated to be approximately 7.1 ± 0.32 cm^3/m at the Haima cold seep vent site, 21.8 ± 0.31 cm^3/m at the Site F, and 3.7 ± 0.22 cm^3/s at the Lingshui site (Fig. S-8). Even considering the rapid decomposition rate that occurred at the third stage, the ROV retained some of the hydrate when it rose to the water surface. The EGHs can significantly enhance the survival of methane bubbles. The EGHs easily form in the cold seep areas on the seafloor, in shallow surface sediments, beneath authigenic carbonate rocks, or even in an empty mussel shell (Fig. S-9). Given the abundance of active cold seep vents worldwide, the potential environmental impact caused by the ascent and subsequent decomposition of EGHs carrying methane bubbles cannot be ignored.

Conclusions

Here, we provide the first record of the destabilising ascent of EGHs. The evolutional patterns of EGHs throughout the water depth scale were established, including the gas escape processes, and the specific temperature variations. Notably, the gas escape process occurred throughout all depths in the experiment. At water pressures > 7.05 MPa (depths > 700 m), the first stage of the evolution of EGHs was observed, during which the morphology of EGHs remained stable. Pressures of 7.05–2.59 MPa (depths of 700–257 m) corresponded to the second stage of EGH ascent, during which peripheral hydrate decomposition and internal hydrate growth coexisted. The decomposition of the peripheral hydrates will cause a hysteresis effect on the decomposition of the hydrates. The third stage (2.59–2.16 MPa, 257–214 m) was the period of internal hydrate decomposition. From our *in situ* experiments, it appears that the presence of EGHs results in methane gas influencing the overlying water column or even the atmospheric environment. It can also provide *in situ* data for gas hydrate exploitation to avoid construction-induced block hydrate uplift, which may increase greenhouse gas emissions.

Acknowledgements

This work was supported by the National Natural Science Foundation of China (52001303, 92058206, 42221005, 41822604, 42049582), Strategic Priority Research Program, CAS (XDB42040302), Young Taishan Scholars Program (tsqn201909158), and Key Project of Ocean Research Center, Chinese Academy of Sciences (COMS2020J03).

Editor: Eric Oelkers

Additional Information

Supplementary Information accompanies this letter at https://www.geochemicalperspectivesletters.org/article2327.

Cite this letter as: Ma, L., Luan, Z., Du, Z., Zhang, X., Zhang, Y., Zhang, X. (2023) The direct observation and interpretation of gas hydrate decomposition with ocean depth. *Geochem. Persp. Let.* 27, 9–14. https://doi.org/10.7185/geochemlet.2327

References

Brewer, P.G., Orr Jr., F.M., Friederich, G., Kvenvolden, K.A., Orange, D.L. (1998) Gas Hydrate Formation in the Deep Sea: In Situ Experiments with Controlled Release of Methane, Natural Gas, and Carbon Dioxide. *Energy & Fuels* 12, 183–188. https://doi.org/10.1021/ef970172q

Case, D.H., Ijiri, A., Morono, Y., Tavormina, P., Orphan, V.J., Inagaki, F. (2017) Aerobic and Anaerobic Methanotrophic Communities Associated with Methane Hydrates Exposed on the Seafloor: A High-Pressure Sampling and Stable Isotope-Incubation Experiment. *Frontiers in Microbiology* 8, 2569. https://doi.org/10.3389/fmicb.2017.02569

Dhamu, V., Qureshi, M.F., Abubakar, S., Usadi, A., Barckholtz, T.A., Mhadeshwar, A.B., Linga, P. (2023) Investigating High-Pressure Liquid CO_2 Hydrate Formation, Dissociation Kinetics, and Morphology in Brine and Freshwater Static Systems. *Energy & Fuels* 37, 8406–8420. https://doi.org/10.1021/acs.energyfuels.3c01089

Dickens, G.R., Quinby-Hunt, M.S. (1994) Methane hydrate stability in seawater. *Geophysical Research Letters* 21, 2115–2118. https://doi.org/10.1029/94GL01858

Du, Z., Zhang, X., Xi, S., Li, L., Luan, Z., Lian, C., Wang, B., Yan, J. (2018) *In situ* Raman spectroscopy study of synthetic gas hydrate formed by cold seep flow in the South China Sea. *Journal of Asian Earth Sciences* 168, 197–206. https://doi.org/10.1016/j.jseaes.2018.02.003

Egger, M., Riedinger, N., Mogollón, J.M., Jørgensen, B.B. (2018) Global diffusive fluxes of methane in marine sediments. *Nature Geoscience* 11, 421–425. https://doi.org/10.1038/s41561-018-0122-8

Hester, K.C., Dunk, R.M., Walz, P.M., Peltzer, E.T., Sloan, E.D., Brewer, P.G. (2007) Direct measurements of multi-component hydrates on the seafloor: Pathways to growth. *Fluid Phase Equilibria* 261, 396–406. https://doi.org/10.1016/j.fluid.2007.07.053

Hester, K.C., Peltzer, E.T., Walz, P.M., Dunk, R.M., Sloan, E.D., Brewer, P.G. (2009) A natural hydrate dissolution experiment on complex multi-component hydrates on the sea floor. *Geochimica et Cosmochimica Acta* 73, 6747–6756. https://doi.org/10.1016/j.gca.2009.08.007

Kvenvolden, K.A. (1988) Methane hydrate — A major reservoir of carbon in the shallow geosphere? *Chemical Geology* 71, 41–51. https://doi.org/10.1016/0009-2541(88)90104-0

Lei, L., Seol, Y., Myshakin, E.M. (2019) Methane Hydrate Film Thickening in Porous Media. *Geophysical Research Letters* 46, 11091–11099. https://doi.org/10.1029/2019gl084450

MacDonald, I.R., Sager, W.W., Peccini, M.B. (2003) Gas hydrate and chemosynthetic biota in mounded bathymetry at mid-slope hydrocarbon seeps: Northern Gulf of Mexico. *Marine Geology* 198, 133–158. https://doi.org/10.1016/s0025-3227(03)00098-7

Mazurenko, L.L., Soloviev, V.A. (2003) Worldwide distribution of deep-water fluid venting and potential occurrences of gas hydrate accumulations. *Geo-Marine Letters* 23, 162–176. https://doi.org/10.1007/s00367-003-0146-x

Pohlman, J.W., Canuel, E.A., Chapman, N.R., Spence, G.D., Whiticar, M.J., Coffin, R.B. (2005) The origin of thermogenic gas hydrates on the northern Cascadia Margin as inferred from isotopic ($^{13}C/^{12}C$ and D/H) and molecular composition of hydrate and vent gas. *Organic Geochemistry* 36, 703–716. https://doi.org/10.1016/j.orggeochem.2005.01.011

Qureshi, M.F., Dhamu, V., Usadi, A., Barckholtz, T.A., Mhadeshwar, A.B., Linga, P. (2022a) CO_2 Hydrate Formation Kinetics and Morphology Observations Using High-Pressure Liquid CO_2 Applicable to Sequestration. *Energy & Fuels* 36, 10627–10641. https://doi.org/10.1021/acs.energyfuels.1c03840

Qureshi, M.F., Khandelwal, H., Usadi, A., Barckholtz, T.A., Mhadeshwar, A.B., Linga, P. (2022b) CO_2 hydrate stability in oceanic sediments under brine conditions. *Energy* 256, 124625. https://doi.org/10.1016/j.energy.2022.124625

Qureshi, M.F., Zheng, J., Khandelwal, H., Venkataraman, P., Usadi, A., Barckholtz, T.A., Mhadeshwar, A.B., Linga, P. (2022c) Laboratory demonstration of the stability of CO_2 hydrates in deep-oceanic sediments. *Chemical Engineering Journal* 432, 134290. https://doi.org/10.1016/j.cej.2021.134290

Rehder, G., Leifer, I., Brewer, P.G., Friederich, G., Peltzer, E.T. (2009) Controls on methane bubble dissolution inside and outside the hydrate stability field from open ocean field experiments and numerical modeling. *Marine Chemistry* 114, 19–30. https://doi.org/10.1016/j.marchem.2009.03.004

Roberts, H.H., Hardage, B.A., Shedd, W.W., Hunt Jr, J. (2006) Seafloor reflectivity—An important seismic property for interpreting fluid/gas expulsion geology and the presence of gas hydrate. *The Leading Edge* 25, 620–628. https://doi.org/10.1190/1.2202667

Sassen, R., Roberts, H.H., Carney, R., Milkov, A.V., DeFreitas, D.A., Lanoil, B., Zhang, C. (2004) Free hydrocarbon gas, gas hydrate, and authigenic minerals in chemosynthetic communities of the northern Gulf of Mexico continental slope: relation to microbial processes. *Chemical Geology* 205, 195–217. https://doi.org/10.1016/j.chemgeo.2003.12.032

Suess, E. (2014) Marine cold seeps and their manifestations: geological control, biogeochemical criteria and environmental conditions. *International Journal of Earth Sciences* 103, 1889–1916. https://doi.org/10.1007/s00531-014-1010-0

Thornton, B.F., Geibel, M.C., Crill, P.M., Humborg, C., Mörth, C.-M. (2016) Methane fluxes from the sea to the atmosphere across the Siberian shelf seas. *Geophysical Research Letters* 43, 5869–5877. https://doi.org/10.1002/2016gl068977

Waite, W.F., Ruppel, C.D., Boze, L.-G., Lorenson, T.D., Buczkowski, B.J., McMullen, K.Y., Kvenvolden, K.A. (2020) Preliminary global database of known and inferred gas hydrate locations. *U.S. Geological Survey data release*. https://doi.org/10.5066/P9LLFVJM

Warzinski, R.P., Lynn, R., Haljasmaa, I., Leifer, I., Shaffer, F., Anderson, B.J., Levine, J.S. (2014) Dynamic morphology of gas hydrate on a methane bubble in water: Observations and new insights for hydrate film models. *Geophysical Research Letters* 41, 6841–6847. https://doi.org/10.1002/2014gl061665

Zeng, X.-Y., Wu, G., Zhong, J.-R., Chen, D.-Y., Sun, C.-Y., Chen, G.-J. (2019) Three-Scale *in Situ* Investigation on the Film Morphology and Mass Transfer Channels during the Thickening Growth of Hydrates on Gas Bubble. *Crystal Growth & Design* 19, 3158–3165. https://doi.org/10.1021/acs.cgd.8b01847

Zhang, X., Du, Z., Luan, Z., Wang, X., Xi, S., Wang, B., Li, L., Lian, C., Yan, J. (2017a) In Situ Raman Detection of Gas Hydrates Exposed on the Seafloor of the South China Sea. *Geochemistry, Geophysics, Geosystems* 18, 3700–3713. https://doi.org/10.1002/2017gc006987

Zhang, X., Du, Z., Zheng, R., Luan, Z., Qi, F., Cheng, K., Wang, B., Ye, W., Liu, X., Lian, C., Chen, C., Guo, J., Li, Y., Yan, J. (2017b) Development of a new deep-sea hybrid Raman insertion probe and its application to the geochemistry of hydrothermal vent and cold seep fluids. *Deep Sea Research Part I: Oceanographic Research Papers* 123, 1–12. https://doi.org/10.1016/j.dsr.2017.02.005

Zheng, J., Chong, Z.R., Qureshi, M.F., Linga, P. (2020) Carbon Dioxide Sequestration via Gas Hydrates: A Potential Pathway toward Decarbonization. *Energy & Fuels* 34, 10529–10546. https://doi.org/10.1021/acs.energyfuels.0c02309

Zhong, J.-R., Zeng, X.-Y., Zhou, F.-H., Ran, Q.-D., Sun, C.-Y., Zhong, R.-Q., Yang, L.-Y., Chen, G.-J., Koh, C.A. (2016) Self-preservation and structural transition of gas hydrates during dissociation below the ice point: an *in situ* study using Raman spectroscopy. *Scientific Reports* 6, 38855. https://doi.org/10.1038/srep38855

Geochemical Perspectives Letters

The direct observation and interpretation of gas hydrate decomposition with ocean depth

L. Ma, Z. Luan, Z. Du, X. Zhang, Y. Zhang, X. Zhang

Supplementary Information

The Supplementary Information includes:

- Methods
- Supplementary Table S-1
- Supplementary Figures S-1 to S-9
- Supplementary Videos S-1 to S-4
- Supplementary Information References

Methods

Field Deployment

The experiments were conducted using the ROV Faxian on the research vessel (RV) "KEXUE" of the Institute of Oceanology, Chinese Academy of Sciences. The experiments were conducted with four pan-tilt 10× zoom HDTV cameras mounted on the ROV Faxian. The real-time temperature and pressure parameters of the surrounding seawater were obtained with a conductivity-temperature-depth (CTD, SBE 25 plus; temperature range: −5 to +35 °C, ±0.001 °C; depth limit 6800 m) sensor on the ROV. Continuous Raman spectra of the EGHs during the ascent process were acquired through a Raman insertion probe (RiP) system installed on an open tool-carrying structure mounted below the ROV Faxian. The system was controlled and communicated with via the umbilical cable of the ROV Faxian.

The RiP system included a 532 nm doubled diode-pumped Nd: YAG laser (ULA-532-100 Invictus®, KOSI), a custom-designed Raman spectrometer (N-RXNE-532-RA-SP, KOSI), and a charge-coupled device (CCD, 1024 × 256 pixel resolution, Andor Technology). The spectrometer and necessary electronic components for the communication power supply and controls were installed inside a titanium pressure chamber with a depth rating of 4500 m. A customized oil-filled optical fibre cable mounted on the outside of the titanium chamber was used to connect the Raman insertion probe for Gas hydrate (RiP-Gh) (Zhang *et al*., 2017a, 2017b). RiP-Gh is an improved new version of the deep-sea Raman insertion Probe (RiP), designed specifically for the collection of solid-translucent samples (Zhang *et al*., 2017b; Du *et al*., 2018). RiP-Gh can directly touch or insert itself into gas hydrate samples. The focal point of the laser beam was designed to enter approximately 3 mm inside the volume of each gas hydrate sample, which allowed for the removal of interference caused by the surrounding seawater from the measured Raman signal.

Experimental Field Conditions

The SCS contains numerous sizable petroliferous basins. High rates of sedimentation in the SCS facilitate the creation of natural gas hydrate formations, and the presence of complex bottom faults or diapiric structures provides ideal conditions for gas transport (Hu *et al*., 2013; Zhang *et al*., 2019, 2020). The experiment was conducted in the Haima, Lingshui, and Site F cold seep areas in the SCS. The Site F cold seep is located on the northern continental slope of the SCS, with a 1100 m water depth and 3.57 ℃ water temperature. Previous *in situ* detection studies have reported the existence of EGHs in the Site F area (Zhang *et al*., 2017a).

The Haima cold seep is located at a depth of 1509 m and has a temperature of 2.88 ℃. The Lingshui cold seep is a newly discovered vent with strong eruption characteristics at a water depth of approximately 1760 m, with a temperature of 2.56 ℃ (Table S-1). The Lingshui and Haima cold seeps are both located at the boundary of the Qiongdongnan Basin. Because of the thick organic-rich Cenozoic strata and the development of pathways for gas migration (consisting of faults and mud diapirs), the Qiongdongnan Basin is rich in natural gas hydrates (He *et al*., 2015; Fang *et al*., 2019). Notably, we investigated each cold seep vent with RiP-Gh before simulating the formation of EGHs (Fig. S-1).

Sample Preparation and *In Situ* Detection

In situ hydrate samples were formed in a cylindrical optical glass cell of approximately 9.4 L (30 cm × 20 cm, L × ⌀) in volume. The upper end of the cell was sealed with a specially made rubber gasket, which simulated natural media such as carbonate rocks and empty shells. The bottom end of the cell was exposed to the ambient seawater directly, thus creating a semi-closed space. Therefore, the cell could ensure the exchange of materials and energy between the inside and outside of the cell volume. The cell was transported to the seafloor by the ROV Faxian and was used to gather gas bubbles to simulate the formation of EGHs at different cold seeps (Video S-1). The EGHs samples were placed near the seafloor and revisited after different periods of elapsed time for *in situ* detection using Raman spectroscopy (Table S-1). The RiP-Gh probe was held by the left robotic arm of ROV Faxian, acquiring spectral information in real time during the ascent of the EGHs (Videos S-2 to S-4). We controlled the rate of uplift of the ROV in each *in situ* experiment at the same rate (Table S-1). A dissolved oxygen sensor (DOS, JFE RINKO I ARO-USB; with a temperature range of −3 to +45 ℃, ±0.02 ℃) was fastened to the frontend of the RiP-Gh probe to obtain the real-time temperature changes inside the gas hydrate. The DOS was placed at the same horizontal position as the RiP-Gh device to detect the temperature inside the EGHs.

In situ Raman Spectroscopy Data Analysis

GRAM/Al (Thermo Fisher Scientific, Inc., Waltham, USA) software was used to process the Raman spectra from the *in situ* experiments. The two apparent Raman peaks in the EGHs samples collected from the Haima and Lingshui cold seeps can be deconvoluted by performing three Gaussian fitting procedures. The three vibrational modes of methane are the $5^{12}6^2$ large cage vibration (2905 cm^{-1}), the 5^{12} small cage vibration (2915 cm^{-1}), and the gaseous CH_4 vibration (2917 cm^{-1}) (Hester *et al*., 2007; Du *et al*., 2018). There was no water peak observed in the Raman spectra of the Haima and Lingshui EGHs samples, so the dissolved CH_4 ν_1 mode (2912 cm^{-1}) was not considered in the Gaussian fit. However, the Raman spectra at Site F did show an obvious water peak, and the presence of dissolved phase methane was considered (Fig. S-2).

Supplementary Table

Table S-1 Parameters for the *in situ* Experiments.

Location	Depth (m)	Pressure (MPa)	Stationary period in the seafloor (h)	Temperature (°C)	pH	ROV rising rate (m/s)
Haima	1509	15.22	0.5	2.88	-	0.61
Lingshui	1760	17.76	2.6	2.56	7.97	0.63
Site F	1100	11.09	48	3.57	7.69	0.61

Supplementary Figures

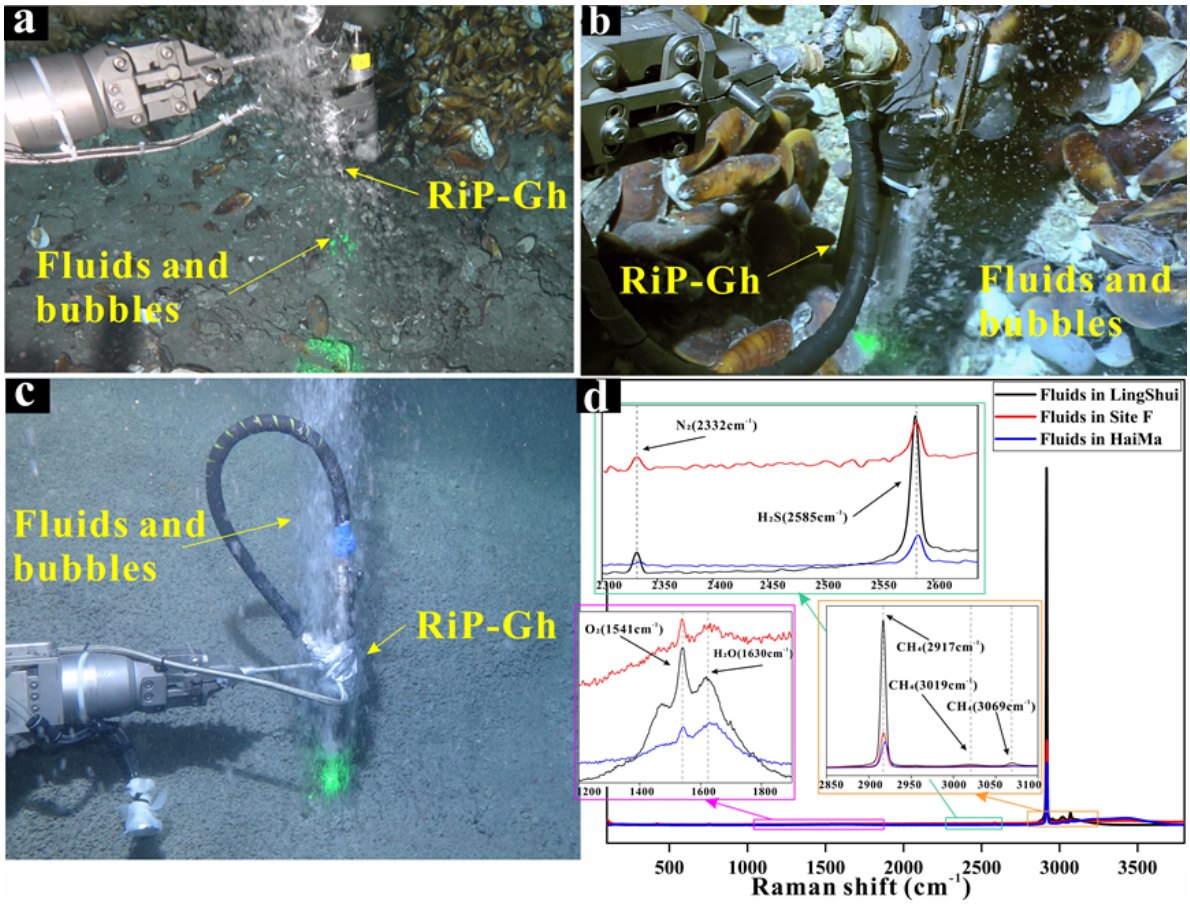

Figure S-1 Insert *in situ* detection of fluids and bubbles erupted from **(a)** Haima, **(b)** Site F and **(c)** Lingshui cold seep vent using RiP-Gh system. **(d)** *In situ* Raman spectra of different cold seep vent.

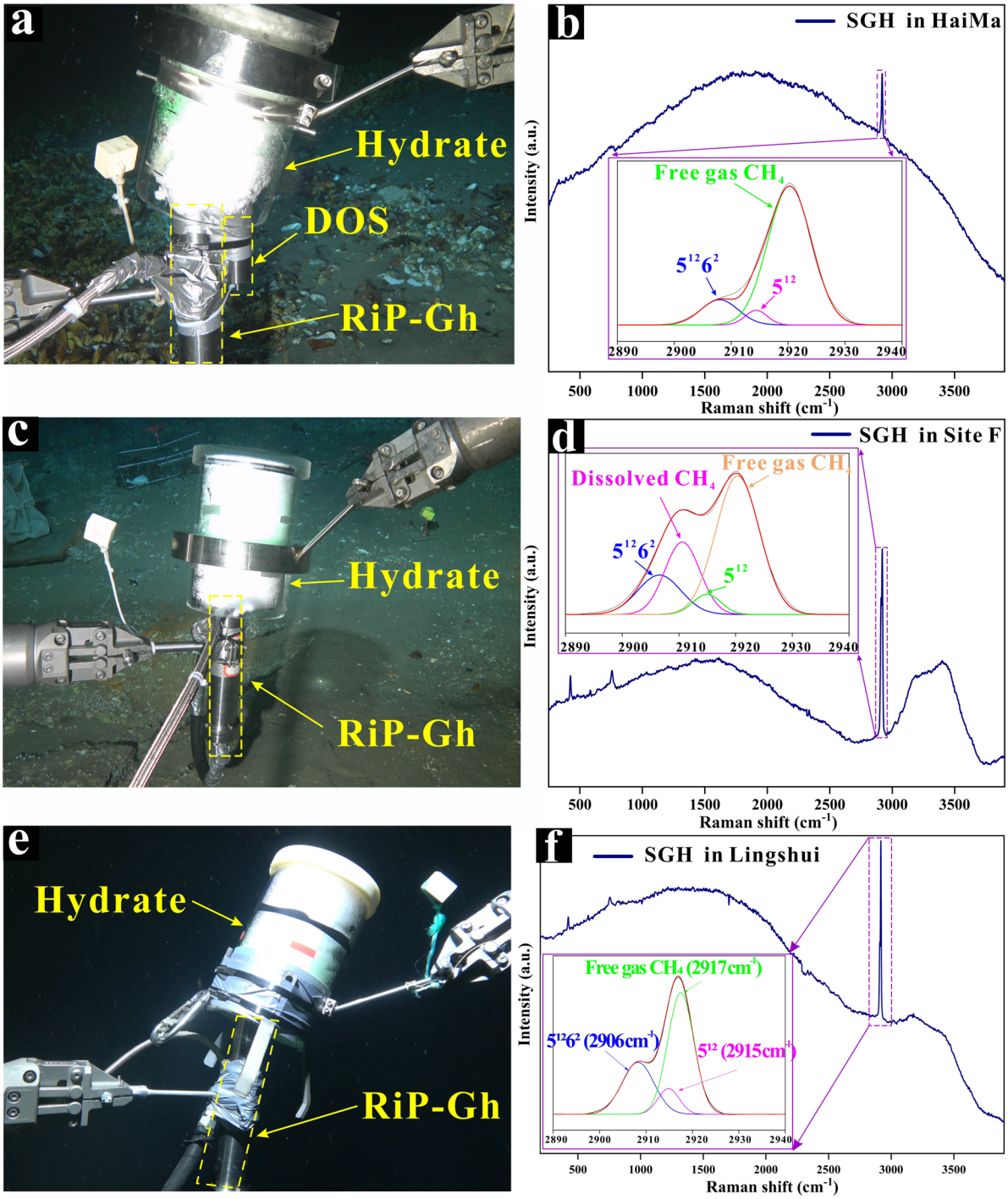

Figure S-2 Fluids and gas bubbles gathered to form the exposed hydrates for in situ detection in **(a)** Haima, **(c)** Site F and **(e)** Lingshui. **(b, d, f)** *In situ* Raman spectroscopy and the deconvolution with Gaussian fit conducted to the two Raman peaks in different cold seep areas.

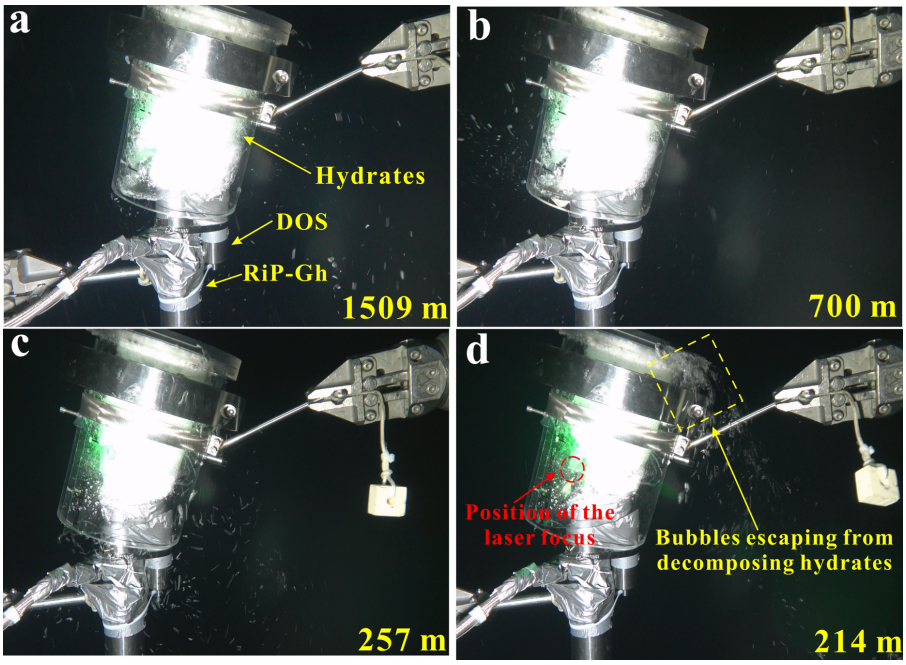

Figure S-3 Images showing hydrate collection and monitoring controlled by the ROV manipulator in Haima *in situ* experiment.

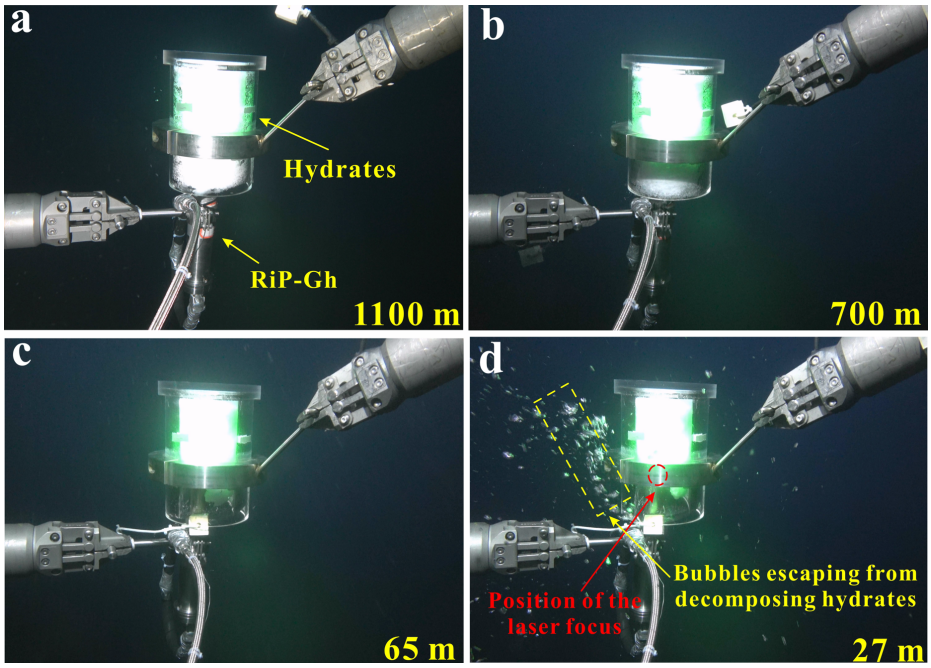

Figure S-4 Images showing hydrate collection and monitoring controlled by the ROV manipulator in Site F *in situ* experiment.

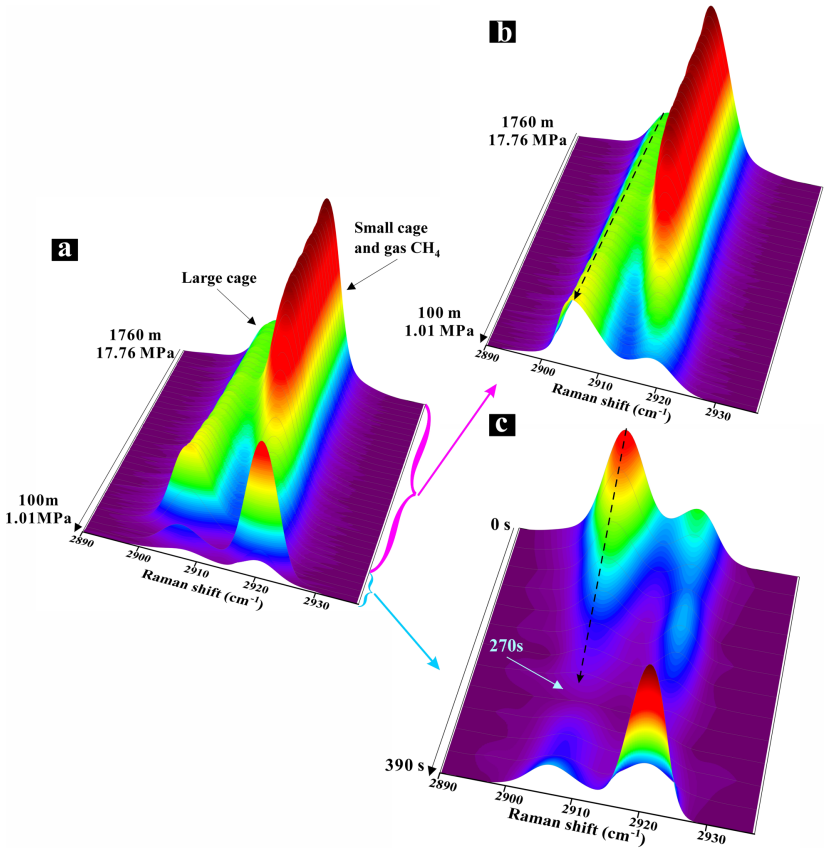

Figure S-5 *In situ* Raman spectra for hydrate samples during ROV uplift in Lingshui. **(a)** ROV overall uplift process, 17.76–1.01 MPa (1760–100 m). **(b)** The stage of continuous growth of 2907 cm^{-1} Raman intensity and continuous decrease of 2917 cm^{-1} Raman intensity. **(c)** Hydrate decomposition stage at the probe starts.

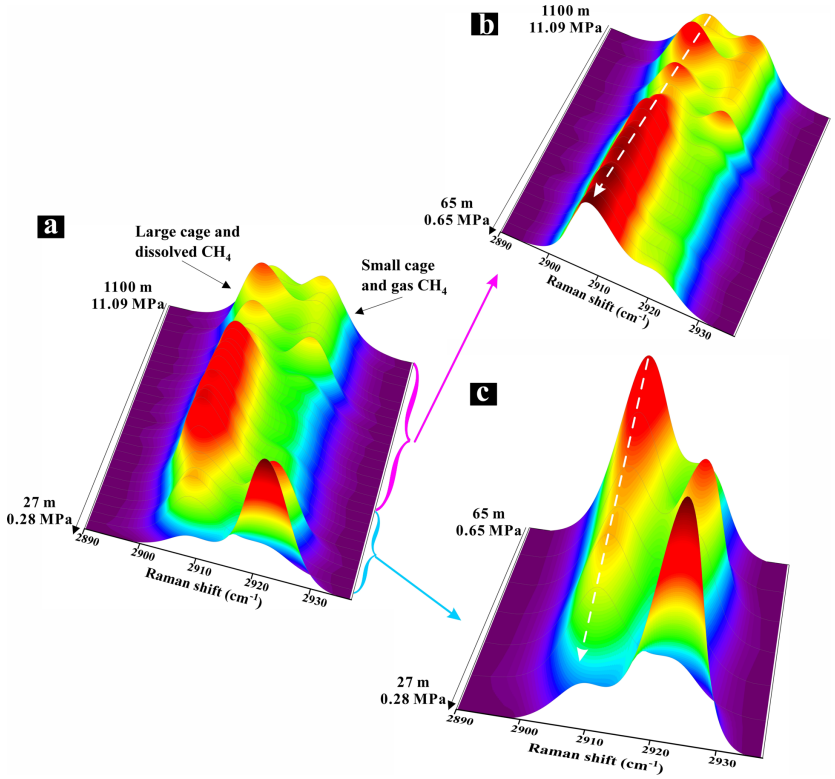

Figure S-6 *In situ* Raman spectra for hydrate samples during ROV uplift in Site F. **(a)** ROV overall uplift process, 11.09–0.28 MPa (1100–27 m). **(b)** The stage of continuous growth of 2907 cm^{-1} Raman intensity and continuous decrease of 2917 cm^{-1} Raman intensity. **(c)** Hydrate decomposition stage at the probe starts.

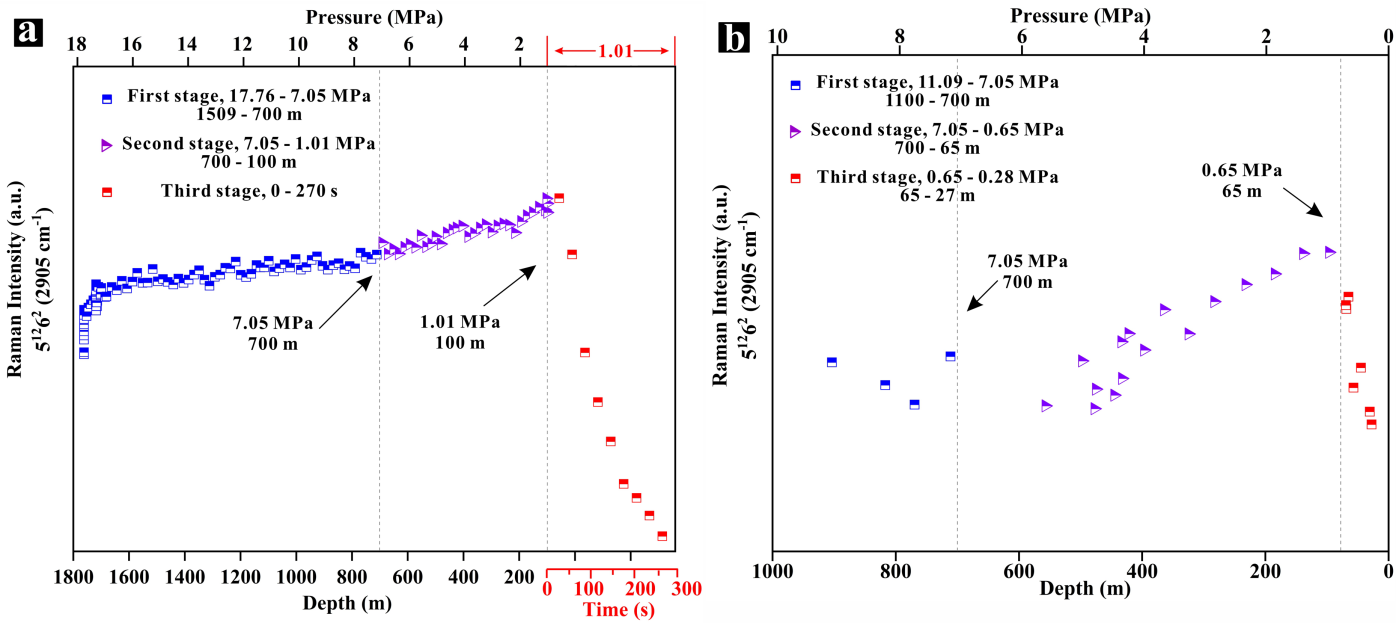

Figure S-7 Variation of large cage Raman intensity with pressure during hydrate uplift in **(a)** Lingshui and **(b)** Site F.

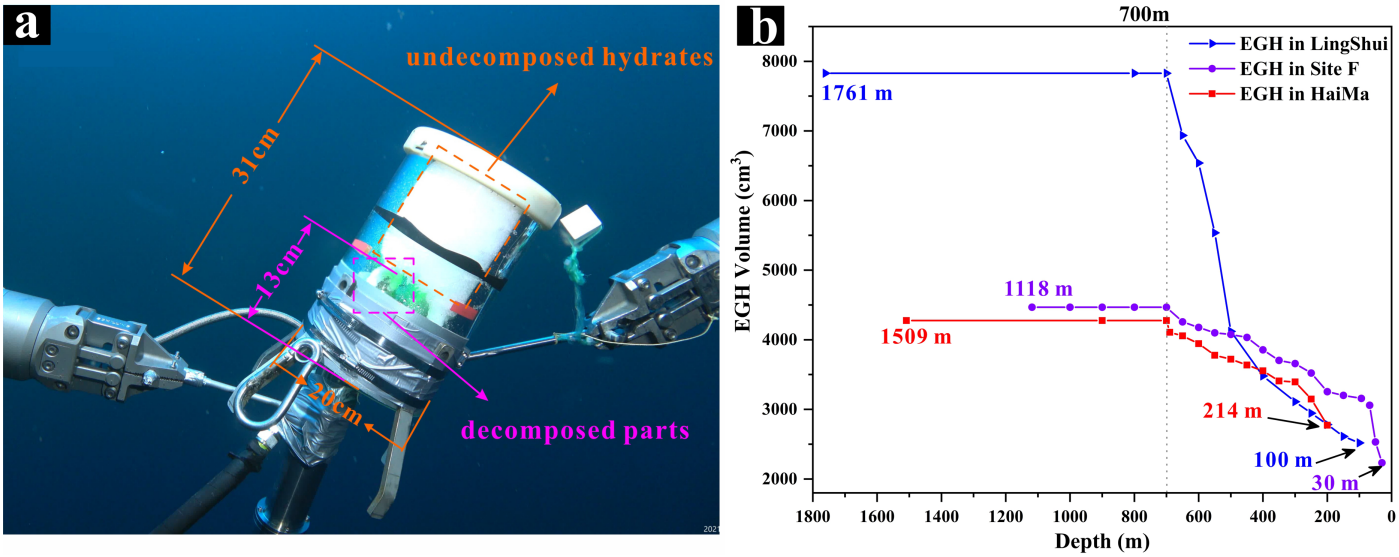

Figure S-8 **(a)** Schematic of EGHs volume estimation. **(b)** Volume variation of EGH with depth during the *in situ* experiments in the Haima cold seep area (the red line), Lingshui cold seep area (the blue line), and Site F cold seep area (the purple line).

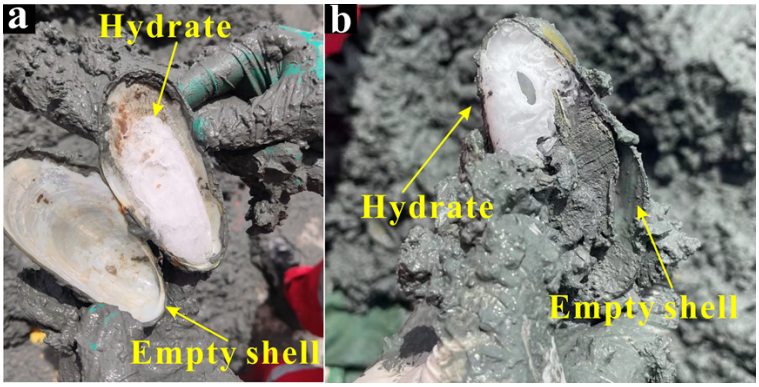

Figure S-9 Exposed gas hydrates formed in empty shells on the seafloor (Haima cold seep area).

Supplementary Videos

The video material provided for this study have all been accelerated.

Video S-1 The formation of EGHs in the Haima, Lingshui, and Site F cold seep area in South China Sea.
Video S-2 *In situ* experiments on the rise process of EGHs in the Haima cold seep area.
Video S-3 *In situ* experiments on the rise process of EGHs in the Lingshui cold seep area.
Video S-4 *In situ* experiments on the rise process of EGHs in the Site F cold seep area.

Videos S-1 through S-4 (.mp4) are available for download from the online version of this article at https://doi.org/10.7185/geochemlet.2327.

Supplementary Information References

Du, Z., Zhang, X., Xi, S., Li, L., Luan, Z., Lian, C., Wang, B., Yan, J. (2018). *In situ* Raman spectroscopy study of synthetic gas hydrate formed by cold seep flow in the South China Sea. *Journal of Asian Earth Sciences* 168, 197–206. https://doi.org/10.1016/j.jseaes.2018.02.003

Fang, Y., Wei, J., Lu, H., Liang, J., Lu, J., Fu, J., Cao, J. (2019) Chemical and structural characteristics of gas hydrates from the Haima cold seeps in the Qiongdongnan Basin of the South China Sea. *Journal of Asian Earth Sciences* 182, 103924. https://doi.org/10.1016/j.jseaes.2019.103924

Hester, K.C., Dunk, R.M., White, S.N., Brewer, P.G., Peltzer, E.T., Sloan, E.D. (2007) Gas hydrate measurements at Hydrate Ridge using Raman spectroscopy. *Geochimica et Cosmochimica Acta* 71, 2947–2959. https://doi.org/10.1016/j.gca.2007.03.032

He, J., Su, P., Lu, Z., Zhang, W., Liu, Z., Li, X. (2015) Prediction of gas sources of natural gas hydrate in the Qiongdongnan Basin, northern South China Sea, and its migration, accumulation and reservoir formation pattern. *Natural Gas Industry* 35, 19–29.

Hu, B., Wang, L., Yan, W., Liu, S., Cai, D., Zhang, G., Zhong, K., Pei, J., Sun, B. (2013) The tectonic evolution of the Qiongdongnan Basin in the northern margin of the South China Sea. *Journal of Asian Earth Sciences* 77, 163–182. https://doi.org/10.1016/j.jseaes.2013.08.022

Zhang, W., Liang, J., Su, P., Wei, J., Gong, Y., Lin, L., Liang, J., Huang, W. (2019) Distribution and characteristics of mud diapirs, gas chimneys, and bottom simulating reflectors associated with hydrocarbon migration and gas hydrate accumulation in the Qiongdongnan Basin, northern slope of the South China Sea. *Geological Journal* 54, 3556–3573. https://doi.org/10.1002/gj.3351

Zhang, W., Liang, J., Yang, X., Su, P., Wan, Z. (2020) The formation mechanism of mud diapirs and gas chimneys and their relationship with natural gas hydrates: insights from the deep-water area of Qiongdongnan Basin, northern South China Sea. *International Geology Review* 62, 789–810. https://doi.org/10.1080/00206814.2018.1491014

Zhang, X., Du, Z., Luan, Z., Wang, X., Xi, S., Wang, B., Li, L., Lian, C., Yan, J. (2017a) In Situ Raman Detection of Gas Hydrates Exposed on the Seafloor of the South China Sea. *Geochemistry, Geophysics, Geosystems* 18, 3700–3713. https://doi.org/10.1002/2017gc006987

Zhang, X., Du, Z., Zheng, R., Luan, Z., Qi, F., Cheng, K., Wang, B., Ye, W., Liu, X., Lian, C., Chen, C., Guo, J., Li, Y., Yan, J. (2017b) Development of a new deep-sea hybrid Raman insertion probe and its application to the geochemistry of hydrothermal vent and cold seep fluids. *Deep Sea Research Part I: Oceanographic Research Papers* 123, 1–12. https://doi.org/10.1016/j.dsr.2017.02.005